Environmental and Sustainability Indicators 30 (2026) 101209

Contents lists available at ScienceDirect

Environmental and Sustainability Indicators

journal homepage: www.sciencedirect.com/journal/environmental-and-sustainability-indicators

Spatial reconfiguration and drivers of ecological risk in the karst region of China: An integrated GMOP-PLUS-InVEST assessment

Tian Wu [a,b,1], Jiqing Yin [c,1], Kaiyang Hong [d], Xianglei Yang [b], Wenxiang Zhang [a,b,*], Taohui Li [e,f,**]

[a] Yunnan Universities Key Laboratory of Plateau Surface Processes and Environmental Changes, Kunming, 650500, China
[b] Yunnan Key Laboratory of Plateau Geographic Processes and Environmental Change, Faculty of Geographical Science, Yunnan Normal University, Kunming, 650500, China
[c] Yunnan Minzu University, Kunming, 650504, China
[d] Faculty of Forestry and Environment, University Putra Malaysia, Serdang, 43400, Malaysia
[e] Yunnan Key Laboratory of Meteorological Disasters and Climate Resources in the Greater Mekong Subregion, Yunnan University, Kunming, 650504, China
[f] Key Laboratory of Water Cycle and Related Land Surface Processes, Institute of Geographic Sciences and Natural Resources Research, Chinese Academy of Sciences, Beijing, 100101, China

ARTICLE INFO

Keywords:
Karst region
Rocky desertification
Ecological risk
Multi-scenario simulation
GMOP-PLUS-InVEST

ABSTRACT

China's karst ecosystems represent a global hotspot of rocky desertification and ecological vulnerability, posing significant challenges for balancing ecological preservation with socioeconomic development. However, persistent scientific gaps remain in quantifying climate-mediated ecological risk (ER) mechanisms, limiting evidence-based conservation strategies. This study employs an integrated social-environment framework that links ecological conditions with landscape sustainability to examine ER dynamics from 2000 to 2020 in karst region of China. The results reveal a significant shift in ER patterns over this period. High-risk areas ($0.017 \leq$ ERI <0.021) expanded from 14.8% to 19.4%, with the most pronounced increase concentrated in the arid Northwest, indicating a spatial reconfiguration. However, the extensively studied southwestern regions exhibited relative stabilization under ongoing ecological restoration. This spatial reconfiguration is attributed to the compounding effects of water scarcity, sparse vegetation, and intensive human activity on the fragile northwestern ecosystems, whereas extensive ecological restoration projects in the Southwest have enhanced vegetation cover and soil retention, thereby mitigating inherent geological vulnerability. Multi-scenario projection demonstrate that the natural development scenario (NDS) facilitates ecological self-recovery and minimizes future ER, whereas economic prioritization would significantly exacerbate degradation in arid karst region. Crucially, partial least squares structural equation model (PLS-SEM) identifies precipitation ($\beta = -0.190$, $p < 0.001$) as the dominant risk-reducing factor through vegetation-mediated hydrological feedbacks. These findings highlight that contemporary ER is driven more by the synergy of climate pressure and human expansion than by inherent vulnerability, necessitating a critical reevaluation of conservation priorities and region-specific mitigation strategies.

1. Introduction

The karst region is a unique geographical unit with a widespread global distribution, playing a key role in the global carbon cycle through its significant carbon sink function, which coexists with inherent ecological fragility (Song et al., 2017). These landscapes, covering approximately 2.20×10^7 km^2 globally and concentrated in south central Europe, eastern North America, and southwestern China (Sweeting, 2012), develop through the long-term erosion of highly soluble carbonate rocks (e.g., limestone and dolomite), creating distinctive

* Corresponding author. Yunnan Universities Key Laboratory of Plateau Surface Processes and Environmental Changes, Kunming, 650500, China.
** Corresponding author. Yunnan Key Laboratory of Meteorological Disasters and Climate Resources in the Greater Mekong Subregion, Yunnan University, Kunming, 650504, China.
E-mail addresses: wenxiangzhang@gmail.com (W. Zhang), taohui0813@foxmail.com (T. Li).
[1] These authors contributed equally to this work and should be considered co-first authors.

https://doi.org/10.1016/j.indic.2026.101209
Received 5 December 2025; Received in revised form 29 January 2026; Accepted 22 February 2026
Available online 6 March 2026
2665-9727/© 2026 The Authors. Published by Elsevier Inc. This is an open access article under the CC BY-NC-ND license (http://creativecommons.org/licenses/by-nc-nd/4.0/).

habitats of surface and subsurface ecosystems co-evolve (Auler and Smart, 2003; Jiang et al., 2020). However, this high solubility leads to chemical erosion and vulnerability. Challenges such as limited soil water retention capacity, low vegetation coverage (with vegetation carbon density decreasing by 62.0% in severely rocky desertified areas), and soil erosion contribute to the degradation of ecosystem service (ES) functions (John and Smith, 1991; Chang et al., 2024; Wang et al., 2025). As a result, the potential of the carbon sink is declining at an annual rate of 0.8% (Jiang et al., 2022), underscoring the urgent need for its stabilization and regulation.

China is one of the most widely distributed karst regions in the world, with its mainly in Southeast regions (Febles et al., 2009; Xiao et al., 2023). Rapid economic development has intensified competition for resources and altered land use, escalating pressure on these fragile ecosystems (Shirmohammadi et al., 2020; Zhou et al., 2022). Furthermore, rapid urbanization and unsustainable land use are expected to aggravate rocky desertification and elevate associated ecological risk (ER) (Dong et al., 2019). ER refers to the probability and severity of adverse impacts on ecosystem structure and function resulting from environmental pressures. A critical subset is landscape ER, which focuses on risks from changes in landscape pattern, such as habitat fragmentation (Hunsaker et al., 1990). In karst regions, the primary drivers of ER include land use and land cover change (LUCC) and altered precipitation pattern, particularly increased drought frequency and intensity. Their synergistic interactions significantly amplify ecological vulnerability (Tang et al., 2025). However, current studies still associate ER predominantly with the severity of rocky desertification and concentrate on the southwestern China (Luo et al., 2024; Wang et al., 2025), often neglecting the combined effects of LUCC and extreme-climate events. Although rock desertification poses a major ecological challenge in China, karst ecosystems are particularly vulnerable due to their distinctive geological and ecological characteristics. Notably, most research has concentrated on the southwestern karst region, leaving other karst areas under-explored. This gap is especially glaring in light of the dual carbon objectives, for which comprehensive evaluations remain limited (Yang et al., 2025). Therefore, to effectively support the national dual carbon strategy, a systematic assessment of rock desertification phenomena across all karst regions in China is necessary. Such an assessment would help to clarify conservation priorities and inform targeted ecological conservation efforts.

Enhancing terrestrial carbon sinks through vegetation restoration is a central strategy for climate action and sustainable development (Pan et al., 2022). A crucial hidden carbon sink, is strategic importance for regulating terrestrial carbon cycling in the karst regions of China (Lou et al., 2023), yet it releases approximately 4.740 Tg C annually through karstification (Song et al., 2017). In areas experiencing severe rocky desertification, vegetation carbon density is declining at an average rate of approximately 0.8% per year, with a concurrent 48.0% reduction in soil organic carbon stocks (Zhou et al., 2025; Wang et al., 2025). Optimized LUCC patterns enable the significant synergistic potential between ecological restoration and carbon sink enhancement by helping to balance carbon storage (CS) and emissions (Wang and Han, 2021; Li et al., 2023). However, intensifying human interventions in karst regions are altering carbon sink dynamics, which in turn exacerbate the relationship between regional carbon sinks and ecological risks (Lan et al., 2022; Kang et al., 2025). Traditional land use models, such as CLUE-S and FLUS, can simulate spatial changes but fail to quantify the multi-objective synergistic among ecological restoration, carbon sink enhancement and economic growth. This limitation has created a disconnect between “carbon sink enhancement” and “ER management” (Jiang et al., 2017; Jiao et al., 2019; De Hertog et al., 2025). Therefore, there is a clear need to develop a comprehensive framework that integrates LUCC simulation, ES assessment and driving mechanism analysis to reveal the synergistic evolution of carbon sinks and ER in karst systems.

To address the coupling mechanism between LUCC and ER, we develop a multi-scale coupling framework integrating the GMOP-PLUS model for LUCC optimization, the InVEST model for spatial assessment and partial least squares structural equation model (PLS-SEM) to analyze driving mechanisms. This framework integrates LUCC simulations from 2000 to 2020 with ES assessment and ER mechanism analysis. Furthermore, it employs multiple-scenario pathways to project LUCC patterns, ER dynamics and the driving mechanisms for 2030 and 2060. The specific objectives are as follows: (1) predict LUCC under four development scenarios for the years 2030 and 2060; (2) quantify rocky desertification intensity and reveal ecological risk succession patterns in karst region of China during 2000-2020 and 2030-2060; and (3) use PLS-SEM to quantify the effect relationships and contributions among the latent variables that influence ER. This work pioneers a comprehensive modeling approach to disentangle natural–anthropogenic interactions, highlights spatial risk heterogeneity to guide targeted conservation and sustainable development in karst ecosystems.

2. Data and methods

2.1. Study area

China is the largest karst region in the world, with an area of 3.44×10^6 km^2, accounting for more than 1/3 of its total land area (Ford and Williams, 1989) (Fig. 1). The karst region is characterized by complex terrain, with an average elevation ranging from 0.80×10^3 to 1.00×10^3 m (Long et al., 2024). It spans multiple climatic zones, including tropical monsoons, sub-tropical humid monsoons and temperate semi-humid climates. Owing to the strong uplift of the eastern edge of the Qinghai-Tibet Plateau, a vertical climate zone spectrum from low-altitude tropics to alpine cold and humid zones. This results in significant climatic and topographic gradients, mainly including mountain, plateau and basin types (Hu et al., 2020; Han et al., 2025). The soil formation rate in China's karst region is extremely slow, and the thin soil layer combined with steep slopes result in a fragile soil ecosystem and low land productivity (Deng et al., 2020). The land use types in this region are mainly sloping cultivated land, sparse forestland, grassland and rocky desertification bare rock land. While cultivated land occupies a high proportion, its productivity is low, with a per unit area yield of less than 30.0% of that in plain regions (Wang et al., 2025).

2.2. Research framework

This study employs a multi-scale analytical framework that integrates interannual, climatic zone, and pixel scales. First, the GMOP-PLUS model was applied to evaluate LUCC data from 2000 to 2020, which is categorized into six land use types: cultivated land, forestland, grassland, water, construction land and unused land. Meanwhile, the model simulated potential LUCC changes under four development scenarios: the natural development scenario (NDS), economic development scenario (EDS), ecological protection scenario (EPS) and comprehensive development scenario (CDS) for the years 2030 and 2060. Additionally, the InVEST model was used to calculate the ES under various development scenarios for 2010-2020, 2030 and 2060. These ES included habitat quality (HQ), soil retention (SR), CS and grain yield (GY). Finally, by measuring the ER in each scenario, this study identifies the primary factors influencing regional ER and their underlying mechanisms using PLS-SEM (Fig. 2).

2.3. Data sources

The study area is categorized into five distinct climatic zones: tropical, sub-tropical, temperate, boreal, and sub-boreal, based on the map of China's climate zoning from the Peking University Geographic Data Platform (http://geodata.pku.edu.cn) (Fig. S1). The karst region data was from NASA MODIS satellite data (https://ladsweb.modaps.cosdis.

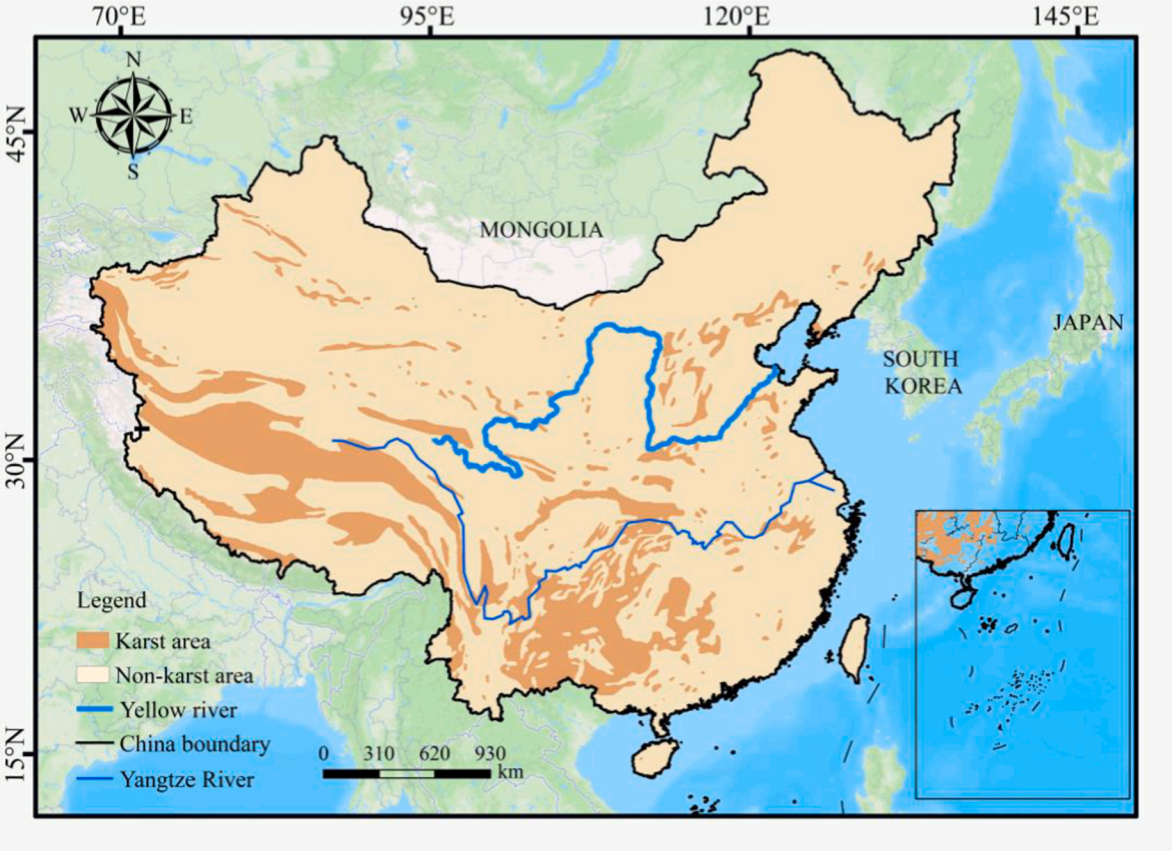

Fig. 1. Spatial distribution map in karst region of China (Based on Long et al., 2024).

nasa.gov) in 2000-2020, with a spatial resolution of 500 m. The normalized difference rock index was calculated based on shortwave infrared and red bands, while the dimidiate pixel model was employed to estimate rock exposure rate and fractional vegetation cover, with corresponding weights determined to obtain the results. Fractional vegetation cover was used the normalized difference vegetation index (NDVI) products provided by global amr surveillance system. Furthermore, the analytic hierarchy process was employed to ascertain indicator weight and construct a comprehensive desertification index in the karst region of China (Long et al., 2024).

Based on existing research (Febles et al., 2009; Huang et al., 2023), this study employs 13 indicators that encompass natural, socioeconomic and spatial accessibility factors (Table S1). These key indicators combine multiple variables that are widely acknowledged in the existing literature and bear a close relation to LUCC and ER impacts. The study utilizes a 0.30×10^2 m resolution land use dataset from 2000 to 2020 provided by the data center for resource and environmental sciences at the Chinese Academy of Sciences. These data are subsequently reclassified into six land use types using ArcGIS 10.8 software (Bi et al., 2024). Prior to analysis, all raster data underwent standardized preprocessing through resampling methods to achieve a uniform spatial resolution of 1 km and were transformed into the same projected coordinate system (WGS_1984_UTM_Zone_50 N), ensuring spatial comparability of data and consistency in model input requirements.

2.4. Methods

2.4.1. GMOP-PLUS model

This study employs the grey multi-objective dynamic programming (GMOP) model, which integrates economic and ecological benefit coordination principles. Four scenarios (NDS, EDS, EPS, and CDS) are established (Table S2) (Liu et al., 2022). The PLUS model integrates Markov chain quantity prediction, enhances CA spatial distribution simulation and combines the LEAS and CARS models for comprehensive analysis (Kowarik and von der Lippe, 2018). The Markov chain predicts land use demand under the NDS scenario for 2030 and 2060. The LEAS module scrutinizes land use data from 2000 to 2020, computing the expansion probability for various land types. The CARS module analyzes the land use cost matrix with neighbourhood weights to evaluate land use quantity, subsequently generating the land use spatial distribution map and total probability. The calculation formula is as follows:

$$P_{i,k}^{d}(x) = \frac{\sum_{n=1}^{M} I\left(h_n(x) = d\right)}{M} \quad (1)$$

Where, $P_{i,k}^{d}(x)$ represents the developmental probability of locus type k in cell I; the value of d is 0 or 1, where 1 represents a change in land use type to type k and 0 represents no change; x is a vector composed of multiple driving factors is the exponential function of the decision tree; $I(h_n(x) = d)$ represents the site type of the nth calculation; $h_n(x)$ is the land use prediction type of the nth decision tree of the vector; M is the total number of decision trees.

$$P_{O,i,k}^{d=1} = P_{i,k}^{d=1} \times \Omega_{i,k}^{t} \times D_{k}^{t} \quad (2)$$

Where, $P_{i,k}^{d=1}$ represents the overall probability value of land use; $\Omega_{i,k}^{t}$ represents the domain effect of land use type k in cell i; D_{k}^{t} represents the influence required for the future change of land use type.

To evaluate the simulation accuracy of the PLUS model, this study validated the simulation results using the Kappa coefficient and confusion matrix. The 2020 was selected as the validation year. The LUCC for 2020 was simulated using data from 2010, and these simulations were subsequently compared with the observed LUCC for that same year. A confusion matrix was constructed using systematic sampling at a sample

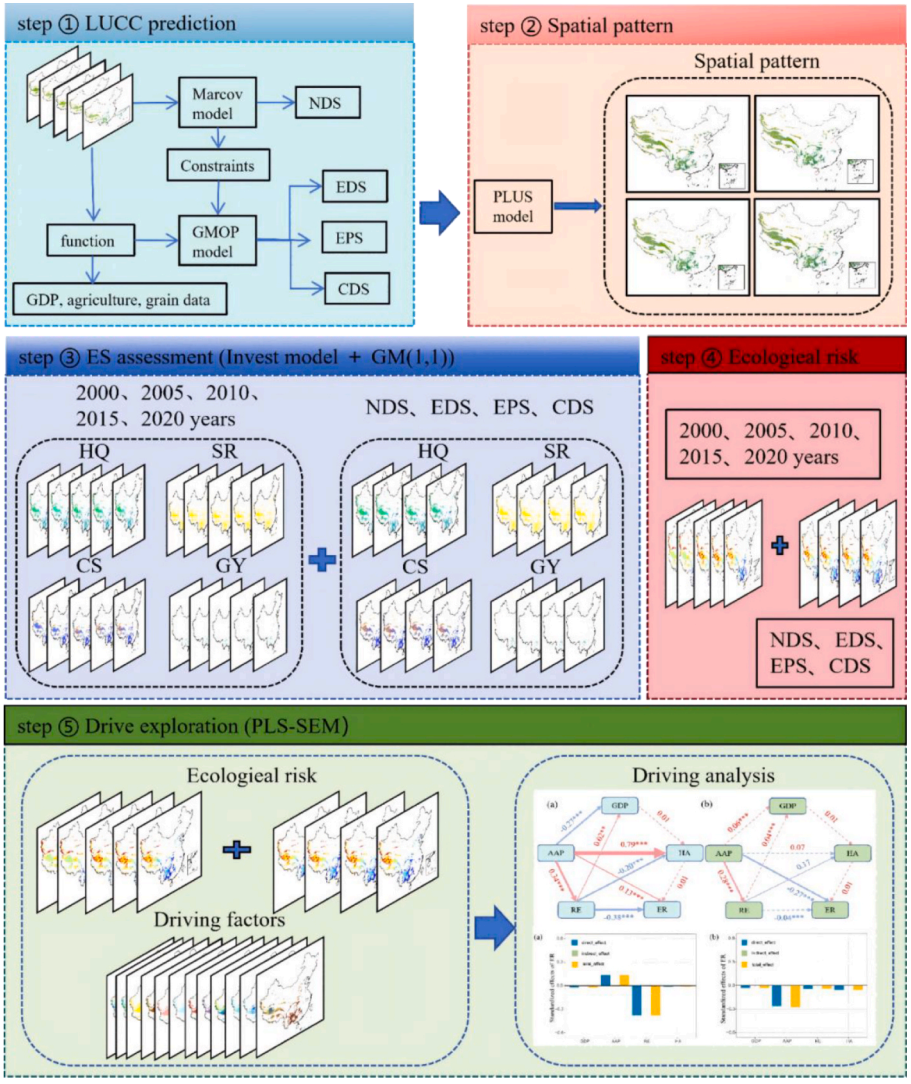

Fig. 2. A coupled modeling framework for ER assessment in karst region of China.

rate of 5.0% (Table S3). The results showed that the overall accuracy of the simulation reached 0.920, and the Kappa coefficient was 0.900, which exceeded the commonly accepted threshold of 0.800. These values indicate that the PLUS model shows good simulation performance in this study and can be applied to multi-scenario LUCC projection.

2.4.2. ES assessment

Based on the current situation in China's karst region, four key ES including HQ, SR, CS and GY are selected (Yang et al., 2024). HQ, SR and CS are realized by the InVEST model, among which GY assessment is assigned according to the proportion of NDVI for cultivated land (Wang et al., 2024). GY is predicted in 2030 by the GM (1,1) model. The calculation formula is as follows:

$$Q_{xj} = H_j \left(1 - \frac{D_{xj}^z}{D_{xj}^z + K^z}\right) \quad (3)$$

Where, Q_{xj} is the HQ index; Hj is the habitat suitability of land use type j; K is the half-saturation constant, set to 0.500 in this paper; The value of the normalization constant z takes the default value of 2.500. In accordance with the InVEST manual and related studies (Yang et al., 2024), the threat factor attributes were set (Table S7), LUCC habitat suitability, and sensitivity to the threat index (Table S8).

$$SDR = R \times K \times LS\,(1 - C \times P) \quad (4)$$

Where, R represents the rainfall erosivity factor; K represents the soil erosion rate; LS represents the slope length and slope factor; C represents the vegetation cover management factor; P represents the soil and water conservation measure factor. The coefficients of C and P for different land use types refer to relevant research (Han et al., 2022) (Table S9).

$$CS = C_{above} + C_{below} + C_{soil} + C_{dead} \quad (5)$$

Where, C_{above} and C_{below} respectively represent the aboveground, underground CS and soil; C_{soil} represents the organic matter CS; C_{dead} represents the apoptotic organic matter CS (Wang et al., 2023; Zhao et al., 2025) (Table S10).

$$Pi = \frac{NDVI_i}{NDVI_{sum}} \times P_{sum} \quad (6)$$

Where, P_i is the GY of the i-th pixel; $NDVI_i$ is the NDVI value on the i-th pixel of cultivated land, and $NDVI_{sum}$ is the sum of the NDVI values; P_{sum} is the total grain output in the current year.

2.4.3. ER assessment

Land use changes are often accompanied by the loss of biodiversity, the decline of ecological service functions and the degradation of eco-

systems, which leads to an increase in regional ER. With reference to previous studies (Wang et al., 2025), this paper carried out ER assessment based on the framework of "risk = loss × probability," as shown in the following equation:

$$ERI_i = \sum_{i=1}^{N} \frac{A_{ki}}{A_K} R_i \quad (7)$$

Where, ERI_i is the ER index of grid i, Ak_i is the area of the i-th type of landscape in grid k; Ak is the area of grid k; R_i is the landscape loss degree index of the i-th landscape type, encompasses key factors such as patch number, fragmentation, and aggregation, reflecting the degree of patch fragmentation and aggregation while directly influencing ecosystem services like HQ, CS, GY, and SR.

$$E_i = a\frac{n_i}{A_i} + b\frac{A}{2A_i}\sqrt{\frac{n_i}{A}} + c\left(\frac{Q_i + M_i}{4} + \frac{L_i}{2}\right) \quad (8)$$

Where, n_i and A_i represent the number of patches and total area of landscape type i; A represents the total area of the landscape; Q_i is the number of quadrats in which patch i appears/total number of quadrats; M_i is the number of patch i/total number of patches; L_i is the area of patch i/total area of the quadrat; a, b, c are the weights of their respective functions (a+b + c = 1).

To capture the spatial pattern changes of ER, referring to related studies (Li et al., 2025), the equidistant reclassification method was used. The ER was categorized into five levels: low-risk ($0.007 \leq ERI < 0.010$), lower-risk ($0.010 < ERI \leq 0.013$), medium-risk ($0.013 \leq ERI < 0.015$), higher-risk ($0.015 \leq ERI < 0.017$), and high-risk ($0.017 \leq ERI < 0.021$).

2.4.4. Multi-scenario land use prediction

The research targets 2030 and 2060 as forecast endpoints, aligning with China's dual carbon goals to assess the phased response characteristics of various development paths concerning territorial spatial patterns, carbon peaking and carbon neutrality goals. The decision variables encompass six major land use types. The objective function was set up as follows: the economic value for 2030 and 2060 uses the GM (1,1) model (Table S4); the maximization of ecological benefits employs the equivalent factor method to account for the ES value, which was combined with grain output value predictions to determine the service value coefficient (Table S5); constraints were established in accordance with the "China Territorial Spatial Planning (2021-2035)" and the primary functional zoning (Yang et al., 2024), implementing land use area restrictions (Table S6). The study ultimately solves the multi-objective optimization through GM (1,1).

The maximum benefit objective function is calculated as:

$$maxZ_i = \sum_{i=1}^{6} C_i X_i \quad (9)$$

$$maxZ_i = 7.08X_1 + 0.67X_2 + 1.71X_3 + 6.20X_4 + 659.93X_5 + 0.0001X_6 \quad (10)$$

The maximum combined benefit objective function is calculated as:

$$maxZ = maxZ_1 + maxZ_2 \quad (11)$$

Where, "max" represents the maximum value of the objective function; "Z_i" is the total value of the target benefits within the study area (ten thousand yuan); "C_i" is the coefficient of the target benefits (ten thousand yuan/hm^2); and "X_i" is the land use type.

2.4.5. PLS-SEM

PLS-SEM is used to estimate the causal relationships between latent variables via measurable variables through a three-level network structure of "observation index-latent variable-system response" (Zhou et al., 2025). In this study, latent variables encompassed three categories: natural conditions (average annual precipitation (AAP), annual average temperature (AAT), soil type (ST), slope (S), elevation model (DEM), rainfall erosion (RE), soil erosion (SE), NDVI), socioeconomic pressures (gross domestic product (GDP), population density (PD)), and spatial accessibility (distance to urban center (DTC), distance to highway (DTH), distance to water system (DTW)). (Table S1). All potential variable data are rasterized (1 km × 1 km) and standardized. The research analysis uses SmartPLS 4.0 and R software to quantitatively analyze the driving path of ER from 2000 to 2020 historical evolution and multi-scenario in 2030 and 2060 and to clarify the direct and indirect impacts (Shi et al., 2024).

3. Results

3.1. Spatio-temporal characteristics of LUCC, ES and ER from 2000 to 2020

3.1.1. Spatio-temporal characteristics of LUCC

Between 2000 and 2020, China's karst regions experienced significant land use and cover changes, characterized by the stability of dominant types and specific conversion pathways (Fig. 3 and Table S11). Cultivated land, forestland, and grassland remained the predominant land types. The most notable changes included a bidirectional transformation between cultivated and construction land, with a net shift of 1.30×10^4 km^2 of cultivated land to construction land, primarily in developing areas, while 3.27×10^3 km^2 of construction land was reconverted to cultivated land. The most significant conversion involved 7.53×10^4 km^2 of grassland transitioning to unused land. Meanwhile, water areas are converted into cultivated land (1.44×10^3 km^2), grassland (3.17×10^3 km^2) and unused land (6.80×10^3 km^2). Spatially, construction land exhibited a distinct expansionary trend, concentrating in eastern coastal regions, the Yangtze River Delta and Pearl River Delta. Water areas were patchily distributed, and unused land was primarily located in the Northwest China and Qinghai-Tibet Plateau. This spatial pattern highlights the strong influence of regional economic development and environmental constraints.

The period from 2005 to 2020 witnessed accelerated land use changes, marked by complex bidirectional exchanges among ecological land types (Fig. 4). Forestland primarily transitioned to cultivated land and grassland, with areas of 8.89×10^3 km^2 and 1.37×10^4 km^2, respectively. Conversely, cultivated land was converted to forestland and grassland covering 8.19×10^3 km^2 and 5.67×10^3 km^2. These reciprocal conversions suggest the simultaneous operation of afforestation programs and agricultural expansion. The large-scale transformation between grassland and unused land, involving 7.53×10^4 km^2 of grassland degradation and 3.96×10^4 km^2 of restoration. These shifts delineate a period of accelerated and competing land use demands.

3.1.2. Spatio-temporal characteristics of ES and ER

Based on the InVEST and GM models, the spatial-temporal dynamics of four key ES (HQ, SR, CS and GY) in China's karst region have been analysed under four scenarios (NDS, EDS, EPS and CDS) from 2000 to 2020 (Fig. 5). HQ maintained relative stability with a pronounced south-north divergence, showing high value in southern China compared to northern regions, and in western regions relative to the east (Fig. 5a). High value HQ areas were concentrated in humid southern regions like the Yangtze River Basin, the Pearl River Basin and the southeast mountainous zones, where a marginal improvement was observed over the two decades. Conversely, the Loess Plateau and northeastern China experienced a relative decline in HQ. SR remained relatively low overall but exhibited a slight increasing trend, with notable enhancement observed within key ecological management zones including the Three-North Shelterbelt and the Loess Plateau Grain-for-Green project (Fig. 5b). CS displayed a clear north-south differentiation (Fig. 5c), marked by substantial augmentation in southern China's tropical and

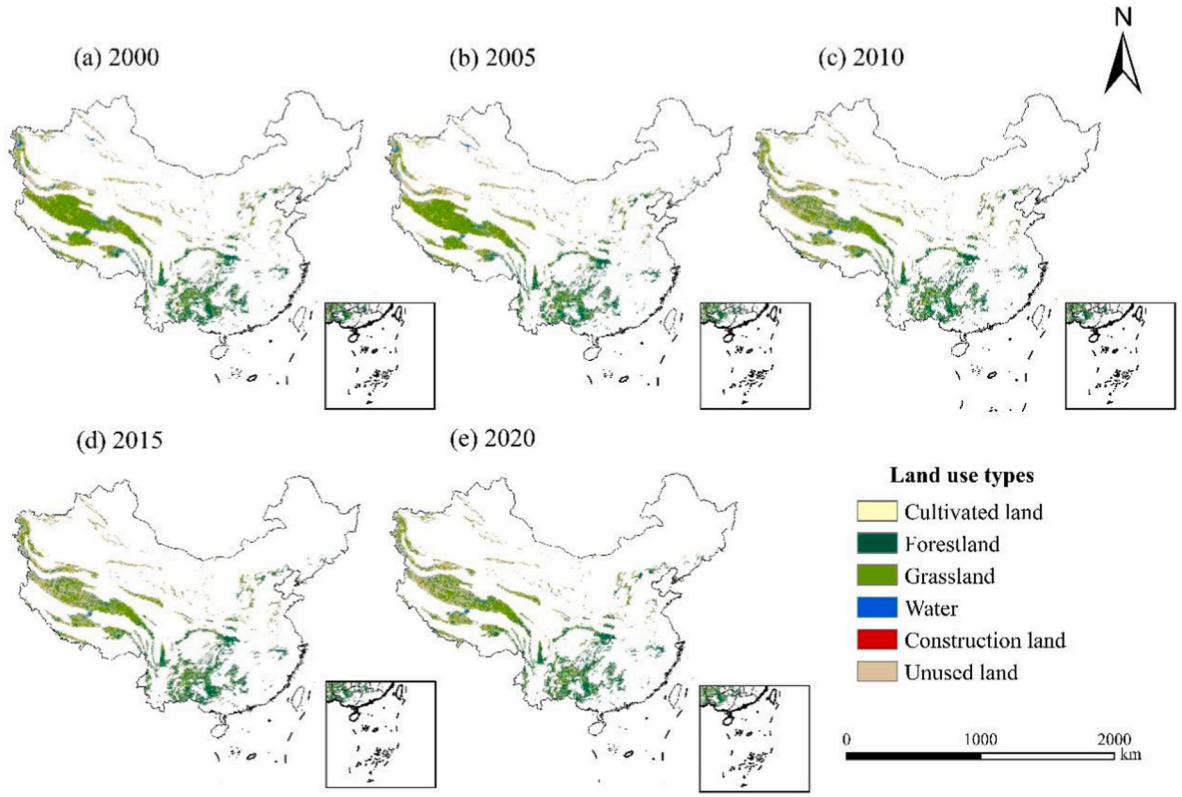

Fig. 3. Spatial characteristics of land use types from 2000 to 2020.

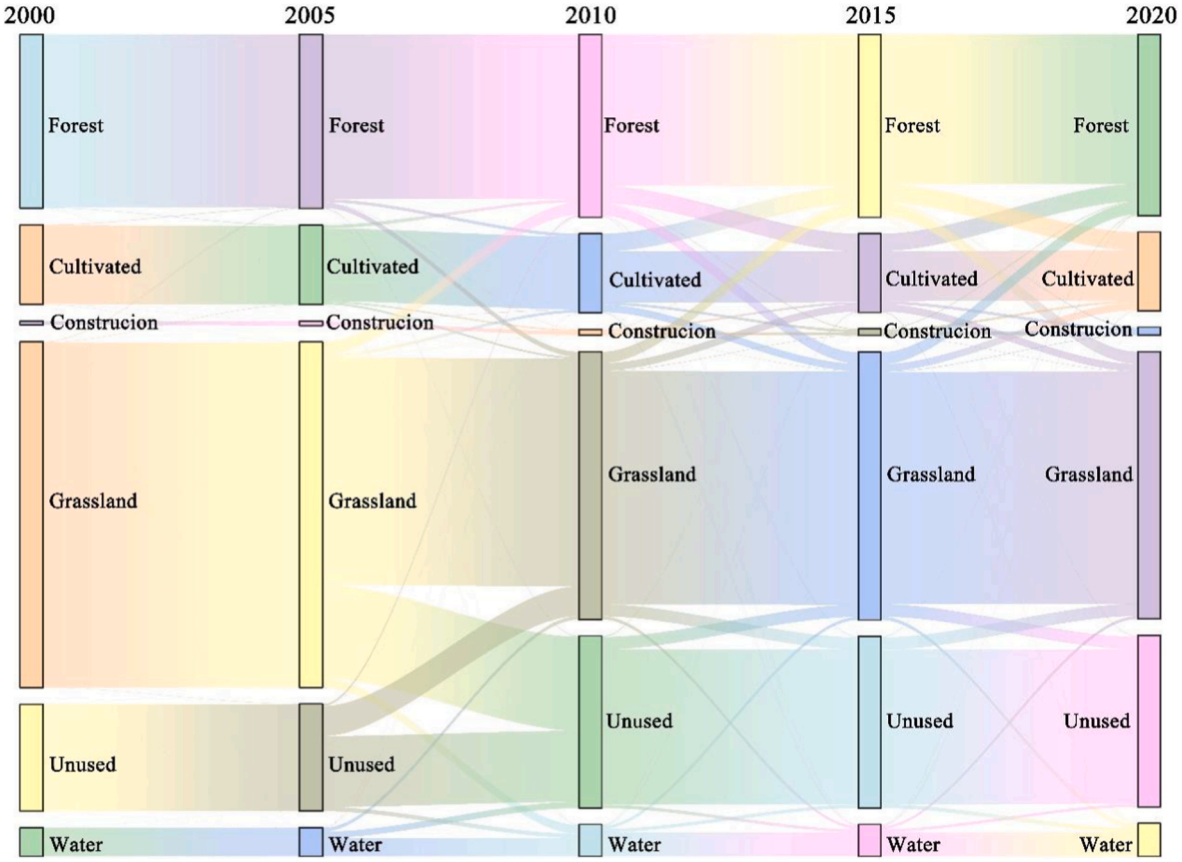

Fig. 4. The Sankey diagram of land use conversion 2000 to 2020.

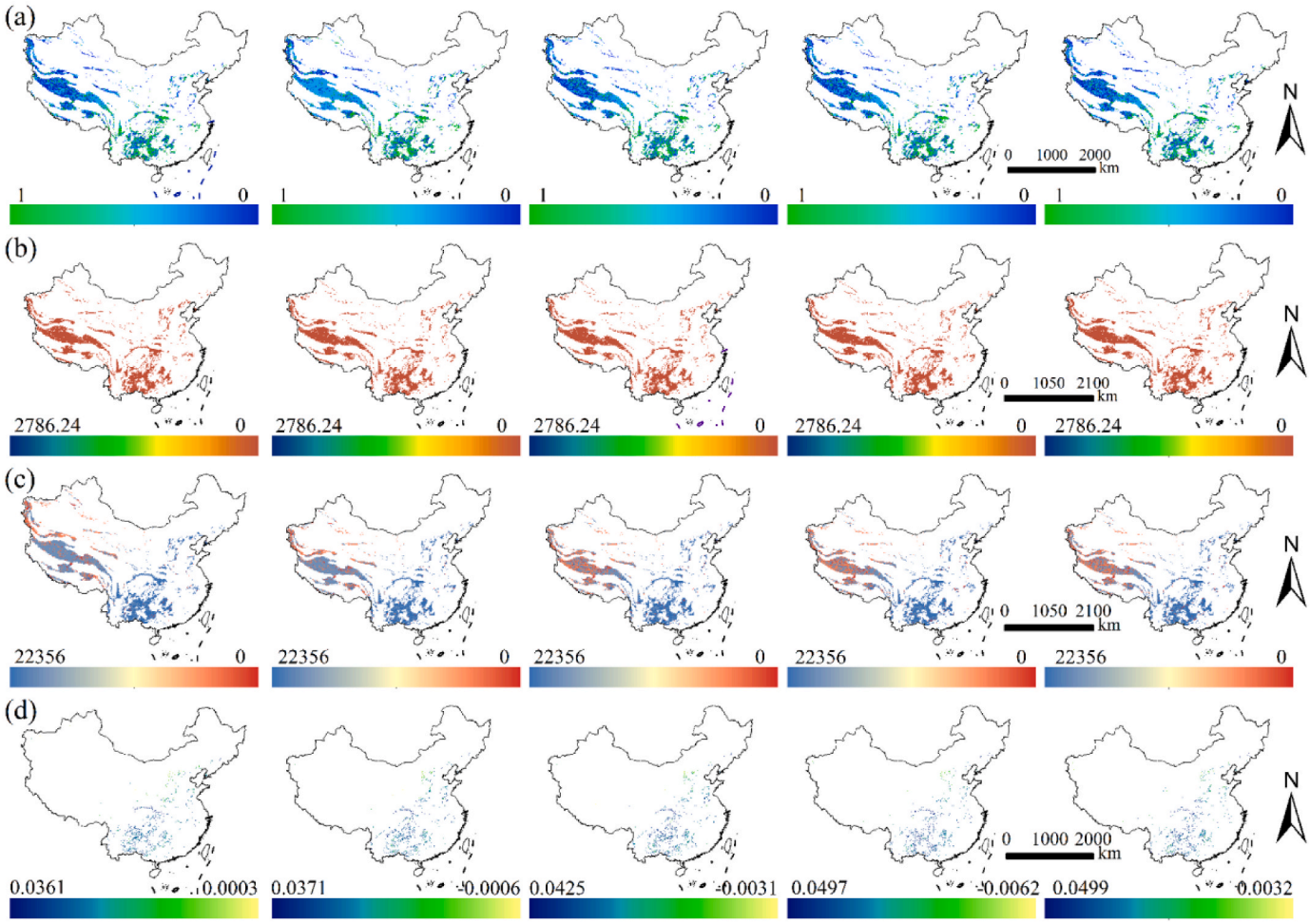

Fig. 5. Spatial characteristics of ES from 2000 to 2020. a-d indicate the 2000-2020 years from left to right. Among, a represents HQ; b represents SR; c represents CS; d represents GY.

sub-tropical forest, contrasting sharply with the limited CS capacity of northwestern deserts and plateaus. A significant reduction occurred specifically in the northwest region in 2010, followed by a period of stability during 2015-2020. GY generally followed a spatial pattern characterized by "increase in core agricultural areas, fluctuation in peripheral regions", displaying higher values in the eastern China and compared to the west (Fig. 5d). Significant increases were noted in the Northeast Plain and North China Plain, while the arid northwest and the Qinghai-Tibet Plateau maintained lower yields.

Significant spatial heterogeneity was observed between 2000 and 2020 (Figs. 6 and 9 and Table S12). During the period of 2000 to 2005, low-risk areas dominated, comprising 26.3% and 24.7% of the region respectively, and were primarily distributed in the humid eastern and southern ecological zones, such as the middle-lower the Yangtze River reaches, South and Southwest China. Sporadic high-risk areas began to emerge in the arid Northwest, including parts of Xinjiang and Tibet. From 2010 to 2020, high-risk areas showed an overall expansion trend, concentrated in arid and semi-arid regions of Northwest China. A localized increase in risk was also observed in parts of East China, often spatially associated with higher-risk areas. Medium-risk areas generally formed transitional zones, adjacent to both higher-risk and lower-risk areas, indicating a spatial correlation in the risk pattern.

3.2. LUCC, ES and ER prediction from 2030 to 2060

3.2.1. LUCC prediction

The results present simulated LUCC patterns across China's karst regions under four development scenarios (NDS, EDS, EPS, and CDS) for 2030 and 2060 (Fig. 7 and Fig. S2). Grassland is projected to maintain the largest spatial extent, followed sequentially by forestland, unused land, cultivated land, water and construction land. The total land use area exhibits an overall increasing trend across both future timeframes under all scenarios. A distinctive pattern emerges in 2030, where unused land represents the only category showing decrease. By 2060, this pattern shifts as both unused land and forestland exhibit reduction. Under the NDS scenario in 2030, both cultivated land and forestland experience decline, while the other three scenarios show progressive expansion of land use areas. Furthermore, the areas particularly notable are the rapid expansion trajectories observed for grasslands, water and construction land across multiple scenarios.

3.2.2. LUCC prediction by ES and ER under different scenarios for 2030 and 2060

Future ES distributions under all scenarios maintain spatial patterns consistent with the 2000-2020 observations, while showing slight enhancement over time (Fig. 8 and Fig. S3). HQ shows improvement in southern regions but declining trends in the northern region, particularly on the Loess Plateau and the North China Plain (Fig. 8a). CS capacity exhibits modest improvement in the northwestern region and the Three-North Shelterbelt, although overall changes remain limited (Fig. 8c).

Significant differences in ER are showed across the various scenarios (Fig. 9 and Table S13). In 2030, NDS exhibits the highest risk level with 13.8% of the area classified as high-risk, exceeding EDS (12.4%), EPS

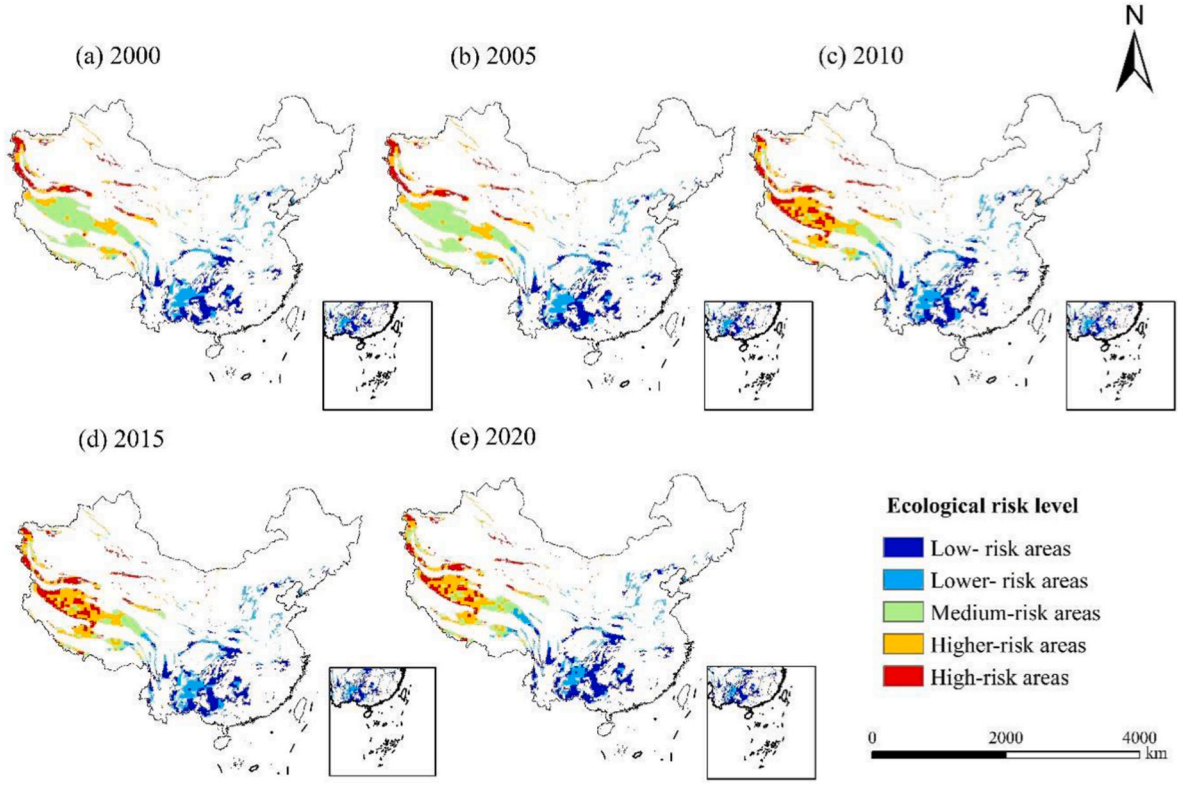

Fig. 6. Spatial characteristics of ER from 2000 to 2020.

(13.4%) and CDS (13.6%). By 2060, EDS shows the highest ER (15.4%) and the lowest NDS (14.6%). ER intensifies under all scenarios from 2030 to 2060. Although the proportion of ER high-risk areas shows minimal variation across scenarios by 2060, these values substantially exceed those of 2030. This consistent upward trend suggests escalating ecological pressure regardless of development pathway, though risk magnitude varies by scenario configuration.

3.3. The complex relationship between ER and environmental factors

Based on the PLS-SEM modeling approach and relevant literature (Qiao et al., 2025; Shi et al., 2024), this study examines the direct and indirect effects of AAP, RE, GDP, and human activities (DTC, DTH and DTW) on the ER index across various climate zones (Fig. 10 and Figs. S4–S6). From 2000 to 2020, the findings reveal that, in addition to the three direct pathways influencing ER, AAP indirectly negatively affects ER through its relationship with RE in the tropical zone (−0.380) (Fig. 10a, Fig. S5a). In the sub-tropical and temperate zones, AAP has a minor indirect effect on ER via GDP (0.060) to HA. However, AAP has a significant negative indirect effect on ER through HA in the temperate zone (−0.430) (Fig. 10b,c and Fig. S5b and c). In the boreal zone, GDP indirectly negatively influences ER (−0.390) because of its impact on HA (−0.310) (Fig. 10d and Fig. S5d). Moreover, AAP indirectly negatively affects ER via its influence on RE in the sub-boreal zone (0.230) (Fig. 10e and Fig. S5e).

In 2030, the indirect negative impact of AAP on ER via its influence on RE (−0.340) is projected to be more pronounced than that from 2000 to 2020 in the tropical zone. This suggests an increase in the adverse effects of natural factors on the ER in these zones. The indirect negative effect of RE on ER is somewhat mitigated by its influence on HA (−0.080) (Fig. S4a and Fig. S-a). In the sub-tropical, temperate and sub-boreal zones, the patterns of path coefficients align with those observed from 2000 to 2020 (Fig. S4b and Fig. S6a). In the boreal zone, GDP indirectly positively affects ER (−0.050) through its impact on HA (−0.310) (Fig. S4d and Fig. S6a).

In 2060, the trend in path coefficients remains consistent with the patterns observed from 2000 to 2020 and in 2030 within the tropical zone. However, AAP has a more pronounced indirect negative influence on ER through its effect on RE (−0.380) in the tropical zone. This suggests that the adverse effects of natural factors on ER in tropical regions will increase in 2060 (Fig. S4f and Fig. S6b). In the boreal zone, GDP indirectly positively impacts ER (−0.100) by affecting HA (−0.310), implying that economic growth in this region may increasingly mitigate the adverse impact on ER over time (Fig. S4i and Fig. S6b). The uniform impacts of natural factors (primarily APP) and HA on ER are evident across all climate zones. When juxtaposing the direct and indirect influences of these drivers on ER from 2000 to 2020, it is evident that the direct effects of natural factors are more dominant.

4. Discussion

4.1. Spatial-temporal patterns of ER under integrated model assessment

The comprehensive evaluation using GMOP-PLUS and InVEST models can effectively elucidate the spatial-temporal differentiation patterns and driving mechanisms of regional ER (Shi et al., 2024; Wang et al., 2025). The integrated assessment reveals pronounced spatial-temporal heterogeneity in LUCC, ES and ER in China's karst region from 2000 to 2020.

From a temporal perspective, LUCC has exhibited a dominant pattern characterized by the expansion of farmland and construction land, coupled with widespread degradation of grassland to unused land. These transitions are associated with intensified soil erosion and reduced CS, thereby increasing the overall ER associated with rocky desertification. This finding aligns with the global consensus that agricultural expansion and urbanization are primary drivers of ecological degradation (Guerrero-Pineda et al., 2022). It further highlights that such human-induced land use transitions may impose particularly severe

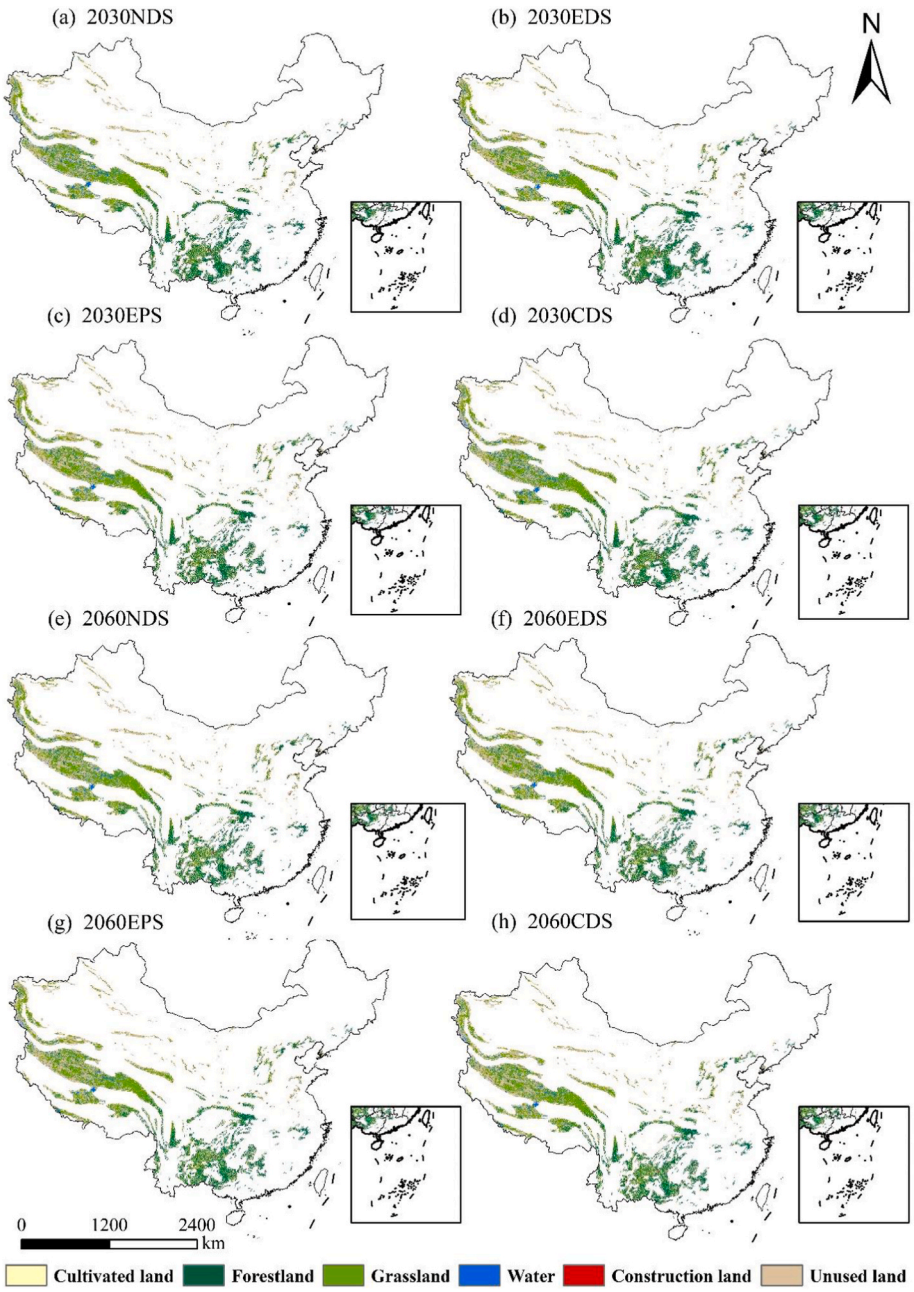

Fig. 7. LUCC prediction under different scenarios in 2030 and 2060.

challenges in ecologically fragile karst regions (D'Ettorre et al., 2024). Spatially, ER displayed marked heterogeneity. High-risk areas showed increasing concentration in the northwestern karst region. In these arid and semi-arid zones, the compounding effects of land degradation and water scarcity appear to elevate risk levels, creating a self-reinforcing cycle of drought vulnerability and ecological stress. Conversely, low-risk areas are mainly distributed in the humid eastern and southern regions. However, localized risk increases were observed even in these regions, largely associated with rapid urban expansion and agricultural intensification.

4.2. Future changes in ER patterns

The findings indicate a fundamental spatial restructuring of risk hotspots in ER pattern, with the key risk area relocating from the extensively studied karst region of southwestern China to the arid Northwest. This spatial reorganization challenges existing paradigms and underscores a critical distinction between inherent geological vulnerability and integrated contemporary ER. The southwestern China maintains high inherent vulnerability due to its soluble carbonate bedrock and steep topography (Febles et al., 2009). However, large-scale national ecological restoration projects, such as farmland-to-forest and grassland conversions (Yu et al., 2025; Wang et al., 2025), alongside a spatially optimized afforestation strategy that reduces forest fragmentation, have effectively buffered ecological degradation and enhanced carbon sequestration and ecosystem resilience (Dong et al., 2026). Despite its geological susceptibility, the region maintained relatively higher HQ and CS during the study period.

In contrast, the karst ecosystems of the arid Northwest maintain a fragile hydrological balance. The combination of sparse vegetation, progressive climatic aridification and expanding economic activities collectively overwhelms the region's natural resilience, particularly agriculture and mining (LeGrand, 1973; Yang et al., 2025). Consequently, the manifest contemporary ER is more acute in the Northwest,

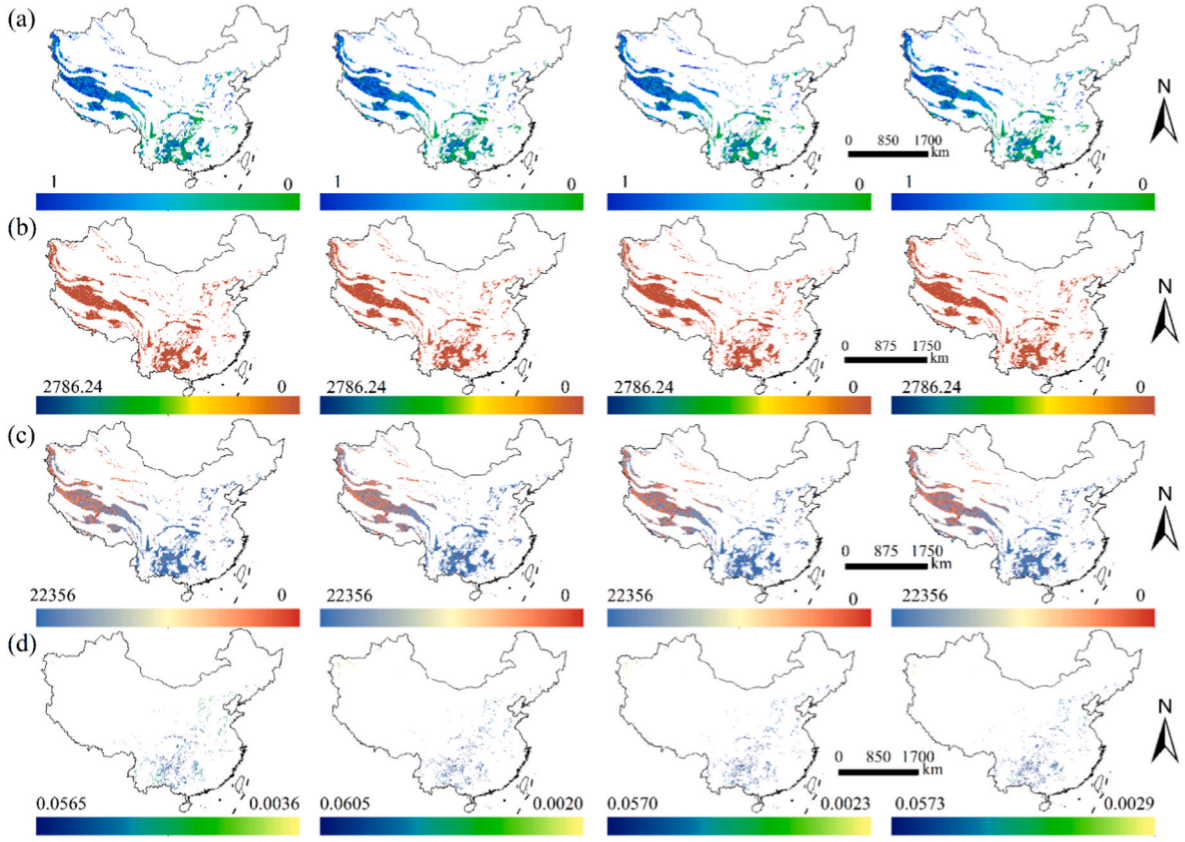

Fig. 8. Spatial characteristics of ES under different scenarios in 2030 (a-d: indicate the spatial distribution of HQ, SR, CS and GY, corresponding to NDS, EDS, EPS and CDS respectively from left to right).

while the inherent geological vulnerability is greater in the Southwest. This heightened risk stems from the synergistic pressures of climate stress and intensive land use acting on a system with low inherent resilience.

Multi-scenario simulations further elucidate how development pathways modulate future risk pattern. A significant reversal in ER emerges between 2030 and 2060. While the NDS initially produces the highest ER in 2030, the EDS exhibits the peak ER by 2060. This shift results from distinct temporal dynamics in human intervention. Under the NDS, high-risk areas expand in the arid Northwest, reinforcing a drought-erosion-risk feedback cycle. Although elevated near-term risks in 2030 may persist due to historical legacies, reducing anthropogenic disturbances in this scenario is expected to promote long-term ecosystem recovery by 2060 (Gong et al., 2024). In contrast, the EDS demonstrates habitat fragmentation and reduced CS in the eastern urban belt, while water resource over-exploitation intensifies erosion risks in the arid northwestern regions (Ding and Jian, 2024; Lu et al., 2025). Despite possible short-term mitigation through technological advances, cumulative economic expansion ultimately leads to the highest long-term risk.

Meanwhile, the EPS promotes CS improvements in the northwestern shelterbelt but may reduce grain yield in the eastern plain, which is consistent with Ren et al. (2022). Notably, the CDS shows the feasibility of the “natal-economy” synergistic pathways. Through optimized land use and management, the CDS achieves concurrent gains in carbon sequestration and grain production across different regions. This balance is crucial for karst regions, where ecological restoration must be integrated with socioeconomic development (Dong et al., 2019).

4.3. Factors driving changes in ER

The PLS-SEM analysis clarifies the complex drivers of ER dynamics in China's karst regions, which are jointly regulated by both natural and anthropogenic factors. The results identify precipitation as a dominant negative driver and human activities as a positive driver of ER, particularly in northwestern regions. Both natural and socio-economic factors influence ER through complex pathways that vary substantially across climate zones. Precipitation indirectly reduces ER intensity by modifying hydrology and soil stability. Precipitation and RE indirectly reduce ER intensity by altering hydrology cycle and soil stability. Reduced precipitation frequently diminishes vegetation coverage and soil moisture, thereby increasing risks in karst landscapes experiencing climate fluctuations (Shao et al., 2024).

Moreover, natural factors directly affect ER intensity across all zones, with direct effects generally exceeding indirect path coefficient. Although natural factors such as precipitation exert direct influences that exceed indirect effects across all climatic zones, their specific mechanisms of action are significantly shaped by regional climate backgrounds. In tropical zone, precipitation directly impacts ER while also indirectly moderating it by suppressing GDP growth and reducing human activities. High rainfall erosivity indirectly reduces ER by diminishing agricultural sustainability through accelerated soil nutrient loss (Deng et al., 2025). However, in sub-tropical and temperate zones, similar precipitation changes may indirectly elevate ER by exacerbating human-water and human-land conflicts (Morris et al., 2025; Zhao et al., 2025). In sub-boreal zone, precipitation indirectly increases ER by reducing rainfall erosivity, potentially due to diminished soil erosion resistance in colder environments (Liang et al., 2024; Wei et al., 2025). Thus, precipitation's direct impact remains predominant though its operational mechanisms vary climatically.

Human activities influence ER primarily through indirect pathways with regional variations. This finding emphasizes that human activities influence ecological security mainly through intermediary processes, such as land use changes and resource consumption rather than through

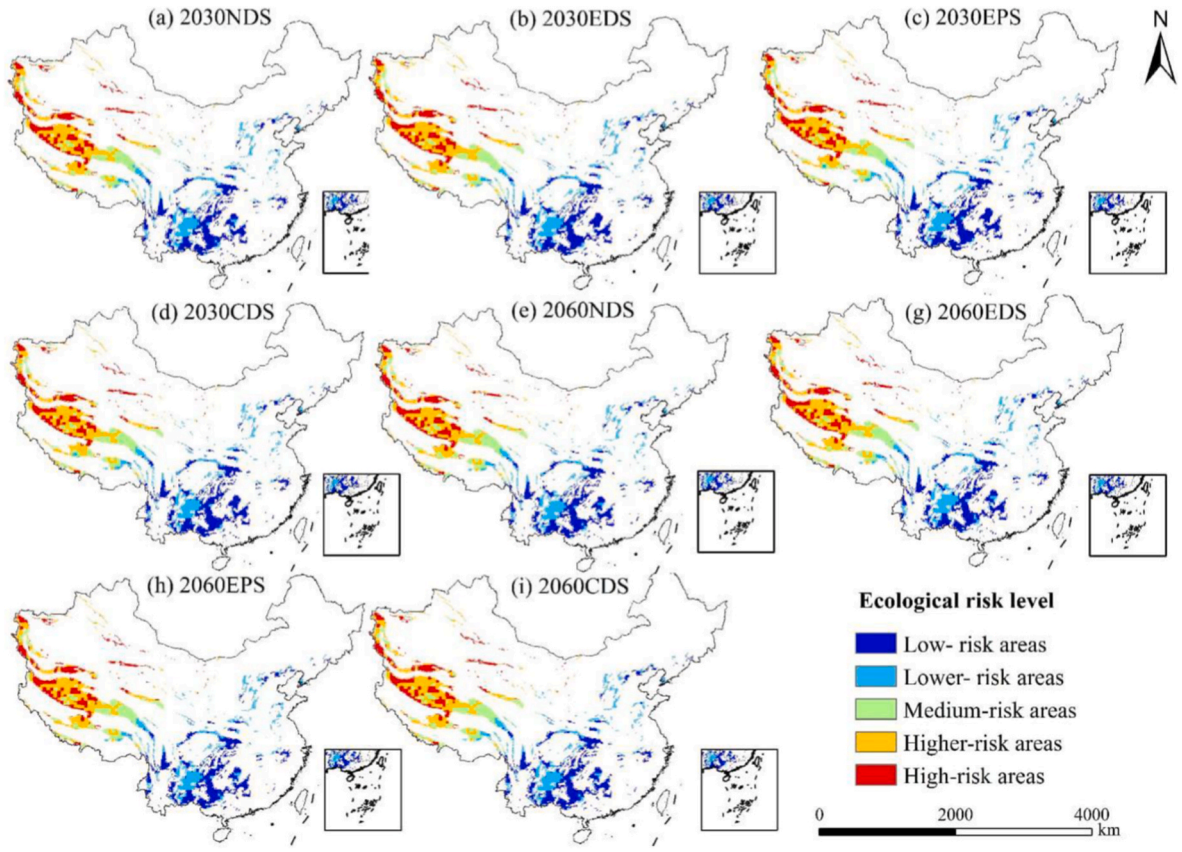

Fig. 9. Spatial characteristics of ER under different scenarios in 2030 and 2060.

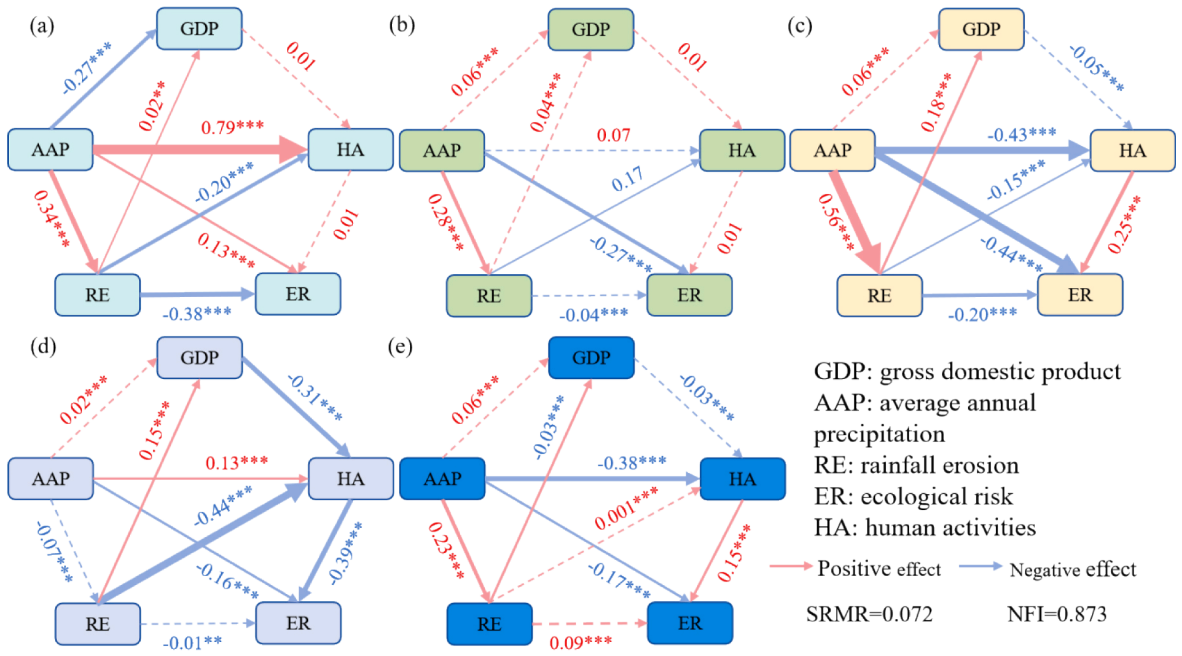

Fig. 10. PLS-SEM for the effects of climate, socioeconomic and HA factors of ER from 2000 to 2020 (a-e: indicate tropical, sub-tropical, temperate, boreal and sub-boreal zones, respectively. Red lines indicate positive effects; blue lines represent negative effects. Numbers near the arrows indicate normalized path coefficients (*$p < 0.05$; **$p < 0.01$; ***$p < 0.001$), and the thickness of the arrows is proportional to the strength of the coefficients. The dashed lines represent weak or non-significant relationships).

direct alterations alone. In tropical zone, human activities are moderated by precipitation and rainfall erosivity, indirectly reducing ER through "passive adaptation to natural stress", which posited by Montfort et al. (2025). In sub-tropical and temperate zones, human activities directly positive increase ER, through irreversible land cover degradation from urbanization and industrialization. In boreal zone,

GDP growth in 2030 and 2060 indirectly elevates ER by promoting human activities, despite potential synergies with ecological protection measures, such as the implementation of ecological compensation (Yun et al., 2024). Critically, the indirect effects of human activities exceed direct influence across all climate zones, indicating that human endeavors either amplify or mitigate ER via complex mediating processes rather than direct action alone.

4.4. Limitations and future studies

This study reveals that natural factors and HA are the primary drivers of ER across different climate zones. However, there are still several limitations should be acknowledged. The assessment framework relies on spatial data at standardized resolutions, which may not fully capture localized heterogeneity in karst terrain characteristics. Parameter selection for ES modeling, while based on established literature, introduces uncertainties in quantitative outputs. The scenario projections assume linear trends in key drivers and do not incorporate potential nonlinear tipping points in ecological responses. Furthermore, the analysis may not fully capture other important dimensions of ER by concentrating on a specific set of ecosystem services. Future research would benefit from higher-resolution terrain data, process-based modeling approaches, and the inclusion of additional ecological indicators to enhance predictive accuracy. Integration of dynamic feedback mechanisms between climate variability and human adaptation strategies would further strengthen the assessment framework.

5. Conclusion

This study pioneers an integrated GMOP-PLUS-InVEST framework to systematically investigate multiscale spatio-temporal coupling mechanisms between natural and anthropogenic interactions in China's karst region. The analysis employs land use scenario simulations and ES-ER synergy diagnostics. Key findings indicate that from 2000 to 2020, land use in China's karst region shows a significant trend characterized by the expansion of farmland and construction land, coupled with the degradation of grassland into unused land. This shift accelerated rocky desertification and led to an expansion of spatial range of ER. The spatial pattern of high-risk areas has been reconfigured, with its hotspot intensifying and expanding in the arid Northwest China. This pattern contrasts with the southwestern karst region, where inherent geological vulnerability remains high but the manifested ER has been mitigated through restoration efforts. This divergence highlights that contemporary ER is increasingly driven by the synergy of climate pressure and human expansion on ecosystems with low resilience.

The multi-scenario simulation results show that the NDS scenario minimizes future ER through the natural vegetation-soil restoration processes, whereas the EDS scenario significantly exacerbates risk in the arid region of Northwest China due to overexploitation of resources. The synergistic effect between ecological services (CS, SR) and risk patterns reveals a potential synergistic path for ecological restoration and risk mitigation. Natural factors and HA are the primary drivers of ER across different climatic zones in the karst region, with AAP as a core natural factor that indirectly mitigates ER by promoting vegetation restoration, whereas HA (DTC) directly exacerbates risks in sub-tropical/temperate zones.

CRediT authorship contribution statement

Tian Wu: Software, Resources, Methodology, Investigation, Formal analysis, Data curation, Conceptualization. **Jiqing Yin:** Project administration, Funding acquisition, Formal analysis, Conceptualization. **Kaiyang Hong:** Visualization, Validation, Supervision, Investigation. **Xianglei Yang:** Visualization, Validation, Investigation. **Wenxiang Zhang:** Writing – review & editing, Writing – original draft, Project administration, Funding acquisition, Formal analysis, Conceptualization. **Taohui Li:** Writing – review & editing, Writing – original draft, Software, Resources, Funding acquisition, Formal analysis, Data curation, Conceptualization.

Declaration of competing interest

The authors declare that they have no known competing financial interests or personal relationships that could have appeared to influence the work reported in this paper.

Acknowledgments

This study was supported by the Yunnan Science and Technology Plan Project (202401AS070638, 202401AU070307 & 202505AS350003) and the National Natural Science Foundation of China (42161017).

Appendix A. Supplementary data

Supplementary data to this article can be found online at https://doi.org/10.1016/j.indic.2026.101209.

Data availability

The datasets generated during and analysed during the current study are publicly available. Data sources and web addresses can be referred to Table S1 in the supporting materials.

References

Auler, A.S., Smart, P.L., 2003. The influence of bedrock-derived acidity in the development of surface and underground karst: evidence from the Precambrian carbonates of semi-arid northeastern Brazil. Earth Surf. Process. Landf. 28, 157–168. https://doi.org/10.1002/esp.443.

Bi, C., Yang, K., Zhang, S., Zeng, W., Liu, J., Rao, Y., Ma, Y., Yang, X., 2024. Simulation and analysis of afforestation potential areas under different development scenarios in Yunnan Province, China. Ecol. Indic. 167, 112695. https://doi.org/10.1016/j.ecolind.2024.112695.

Chang, J., Li, Q., Zhai, L., Liao, C., Qi, X., Zhang, Y., Wang, K., 2024. Comprehensive assessment of rocky desertification treatment in Southwest China karst. Land Degrad. Dev. 35, 3461–3476. https://doi.org/10.1002/ldr.5146.

De Hertog, S.J., Orlov, A., Havermann, F., Guo, S., Manola, I., Pongratz, J., Lejeune, Q., Schleussner, C.F., Menke, I., Humpenöder, F., Popp, A., Lawrence, P., Hurtt, G.C., Chini, L., Vanderkelen, I., Davin, E.L., Reerink, T., Seneviratne, S.I., Verbeeck, H., Thiery, W., 2025. Limited effect of future land-use changes on human heat stress and labor capacity. Earths Future 13. https://doi.org/10.1029/2024EF005021 e2024EF005021.

Deng, Y., Wang, S., Bai, X., Luo, G., Wu, L., Chen, F., Wang, J., Li, Q., Li, C., Yang, Y., Hu, Z., Tian, S., 2020. Spatiotemporal dynamics of soil moisture in the karst areas of China based on reanalysis and observations data. J. Hydrol. 585, 124744. https://doi.org/10.1016/j.jhydrol.2020.124744.

Deng, R., Li, D., Zhao, Y., Walling, D.E., Panagos, P., Borrelli, P., Ciais, P., Huang, Y., Bai, Y., Chalov, S., Golosov, V.N., Fu, X., Miao, C., Wei, J., Ni, J., 2025. Intensified rainfall overrides vegetation greening in driving erosion and carbon loss on the Tibetan Plateau. Sci. Bull. 70, 3698–3702. https://doi.org/10.1016/j.scib.2025.09.005.

D'Ettorre, U.S., Liso, I.S., Parise, M., 2024. Desertification in karst areas: a review. Earth Sci. Rev. 253, 104786. https://doi.org/10.1016/j.earscirev.2024.104786.

Ding, X., Jian, S., 2024. Synergies and trade-offs of ecosystem services affected by land use structures of small watershed in the Loess Plateau. J. Environ. Manage. 350, 119589. https://doi.org/10.1016/j.jenvman.2023.119589.

Dong, N., Liu, Z., Luo, M., Fang, C., Lin, H., 2019. The effects of anthropogenic land use changes on climate in China driven by global socioeconomic and emission scenarios. Earths Future 7, 784–804. https://doi.org/10.1029/2018EF000932.

Dong, Y., Yu, Z., Pugh, T., Agathokleous, E., Zhang, F., Sitch, S., You, W., Han, W., Olin, S., Liu, S., Zhou, G., Cabral, P., Sun, P., 2026. Enhancing carbon sinks in China using a spatially-optimized forestation strategy. Nat. Commun. https://doi.org/10.1038/s41467-026-68288-5.

Febles, J.M., Tolón, A., Vega, M.B., 2009. Edaphic indicators for assessment of soil erosion in karst regions, province of Havana, Cuba. Land Degrad. Dev. 20, 522–534. https://doi.org/10.1002/ldr.929.

Ford, D.C., Williams, P.W., 1989. Karst Geomorphology and Hydrology. Unwin Hyman.

Gong, H., Wang, G., Fan, C., Zhuo, X., Sha, L., Kuang, Z., Bi, J., Cheng, T., 2024. Temporal accumulation and lag effects of precipitation on carbon fluxes in terrestrial ecosystems across semi-arid regions in China. Agric. For. Meteorol. 356, 110189. https://doi.org/10.1016/j.agrformet.2024.110189.

Guerrero-Pineda, C., Iacona, G.D., Mair, L., Hawkins, F., Siikamäki, J., Miller, D., Gerber, L.R., 2022. An investment strategy to address biodiversity loss from agricultural expansion. Nat. Sustain. 5, 610–618. https://doi.org/10.1038/s41893-022-00871-2.

Han, C., Zheng, J., Guan, J., Yu, D., Lu, B., 2022. Evaluating and simulating resource and environmental carrying capacity in arid and semiarid regions: a case study of Xinjiang, China. J. Clean. Prod. 338, 130646. https://doi.org/10.1016/j.jclepro.2022.130646.

Han, Q., Yin, J., Li, T., Chen, J., Shi, Z., Zhang, W., 2025. Integrated isotopic-hydrological method reveals karst plateau reservoir leakage dynamics in urban water systems. J. Hydrol.: Reg. Stud. 62, 102901. https://doi.org/10.1016/j.ejrh.2025.102901.

Hu, Z., Wang, S., Bai, X., Luo, G., Li, Q., Wu, L., Yan, Y., Tian, S., Li, C., Deng, Y., 2020. Changes in ecosystem service values in karst areas of China. Agric. Ecosyst. Environ. 301, 107026. https://doi.org/10.1016/j.agee.2020.107026.

Huang, F., Zuo, L., Gao, J., Jiang, Y., Du, F., Zhang, Y., 2023. Exploring the driving factors of trade-offs and synergies among ecological functional zones based on ecosystem service bundles. Ecol. Indic. 146, 109827. https://doi.org/10.1016/j.ecolind.2022.109827.

Hunsaker, C.T., Graham, R.L., Suter, G.W., O'Neill, R.V., Barnthouse, L.W., Gardner, R. H., 1990. Assessing ecological risk on a regional scale. Environ. Manage. 14, 325–332. https://doi.org/10.1007/bf02394200.

Jiang, W., Deng, Y., Tang, Z., Lei, X., Chen, Z., 2017. Modelling the potential impacts of urban ecosystem changes on carbon 561 storage under different scenarios by linking the CLUE-S and the InVEST models. Ecol. Model. 345, 30–40. https://doi.org/10.1016/j.ecolmodel.2016.12.002.

Jiang, Z., Zhang, C., Luo, W., Xiao, Q., Wu, Z., 2022. Research progress and prospect of carbon sink in karst region of China. Carsol. Sin./Zhong Guo Yan Rong 41, 345–355. https://doi.org/10.11932/karst20220302.

Jiang, Z., Liu, H., Wang, H., Peng, J., Meersmans, J., Green, M.S., Quine, A.T., Wu, X., Song, Z., 2020. Bedrock geochemistry influences vegetation growth by regulating the regolith water holding capacity. Nat. Commun. 11, 2392. https://doi.org/10.1038/s41467-020-16156-1.

Jiao, M., Hu, M., Xia, B., 2019. Spatiotemporal dynamic simulation of land-use and landscape-pattern in the Pearl River Delta, China. Sustain. Cities Soc. 49, 101581. https://doi.org/10.1016/j.scs.2019.101581.

John, G., Smith, D., 1991. Human Impact on the Cuilcagh Karst Areas. Univ. Padova, pp. 23–28.

Kang, Y., Shen, L., Li, C., Huang, Y., Chen, L., 2025. Increased soil multifunctionality is determined by altered bacterial-fungal-protistan compositions and co-occurrence network complexity during vegetation restoration in a Karst region, southwest China. J. Appl. Ecol. 62, 1216–1228. https://doi.org/10.1111/1365-2664.70028.

Kowarik, I., von der Lippe, M., 2018. Plant population success across urban ecosystems: a framework to inform biodiversity conservation in cities. J. Appl. Ecol. 55, 2354–2361. https://doi.org/10.1111/1365-2664.13144.

Lan, X., Ding, G., Dai, Q., Yan, Y., 2022. Assessing the degree of soil erosion in karst mountainous areas by extenics. Catena 209, 105800. https://doi.org/10.1016/j.catena.2021.105800.

LeGrand, H.E., 1973. Hydrological and Ecological Problems of Karst Regions: hydrological actions on limestone regions cause distinctive ecological problems. Science 179, 859–864. https://doi.org/10.1126/science.179.4076.859.

Li, W., Kang, J., Wang, Y., 2025. Exploring the interactions and driving factors among typical ecological risks based on ecosystem services: a case study in the Sichuan-Yunnan ecological barrier area. Ecol. Indic. 170, 113000. https://doi.org/10.1016/j.ecolind.2024.113000.

Li, T., Yin, P., Lv, A., Zhang, W., Yin, J., Xiong, J., Liu, Y., 2023. Spatio-Temporal Characteristics of Climate Production Potential of Vegetation in Eastern Monsoon Region of China, vol. 51. J. North-East For. Univ., pp. 62–69. https://doi.org/10.3969/j.issn.1000-5382.2023.10.011

Liu, X., Liu, Y., Wang, Y., Liu, Z., 2022. Evaluating potential impacts of land use changes on water supply–demand under multiple development scenarios in dryland region. J. Hydrol. 610, 127811. https://doi.org/10.1016/j.jhydrol.2022.127811.

Liang, Q., Zhang, H., Ma, S., Han, Q., Cao, Y., Yang, D., Yin, J., Zhang, W., 2024. Tracing soil erosion history using geochemical signatures in lake sediments: insights from the southeastern Tibetan Plateau margin. Catena 245, 108341. https://doi.org/10.1016/j.catena.2024.108341.

Long, M., Bai, X., Li, Z., Xue, Y., Chen, F., Li, C., Ran, C., Zhang, S., Du, C., Song, F., Xiao, B., Xiong, L., 2024. Positive contribution and negative impact of karst rocky desertification control on biodiversity in southwest China. Acta Geogr. Sin. 79, 97–113. https://doi.org/10.11821/dlxb202401007.

Lou, H., Yang, S., Shi, X., Zhang, J., Pan, Z., Lim, C., Zhang, Y., Zhou, B., Li, H., Shi, Y., Yi, Y., Luo, Y., 2023. Whether the enhanced terrestrial vegetation carbon sink affect the water resources in the middle-low latitude karst areas of China? J. Hydrol. 620, 129510. https://doi.org/10.1016/j.jhydrol.2023.129510.

Lu, C., Zhang, Q., Woolway, R.I, Ma, L., Liu, T., Wang, G., Sun, D., Singh, V.P., Bai, Y., Sun, B., Huang, X., 2025. Global warming will increase the risk of water shortage in Northwest China. Earths Future 13. https://doi.org/10.1029/2025EF006199 e2025EF006199.

Luo, D., Zhou, Z., Zhang, L., Chen, Q., Huang, D., Feng, Q., Wu, T., Wu, L., 2024. Evolution and driver analysis of forest carbon stocks in karst mountainous areas of southwest China in the context of rocky desertification management. Catena 246, 108335. https://doi.org/10.1016/j.catena.2024.108335.

Montfort, S., Callaghan, M., Creutzig, F., Lamb, W.F., Lu, C., Repke, T., Ge, K., Minx, J., 2025. Systematic global stocktake of over 50,000 urban climate change studies. Nat. Cities. 1–13. https://doi.org/10.1038/s44284-025-00260-8.

Morris, J., Sokolov, A., Reilly, J., Libardoni, A., Forest, C., Paltsev, S., Schlosser, C.A., Prinn, R., Jacoby, H., 2025. Quantifying both socioeconomic and climate uncertainty in coupled human-Earth systems analysis. Nat. Commun. 16, 2703. https://doi.org/10.1038/s44284-025-00260-8.

Pan, H., Zhang, M., Cheng, Z., Jiang, H., Yang, J., Wang, P., He, P., Zhou, H., 2022. Carbon-free and binder-free Li-Al alloy anode enabling an all-solid-state Li-S battery with high energy and stability. Sci. Adv. 8. https://doi.org/10.1126/sciadv.abn4372 eabn4372.

Qiao, B., Yang, H., Cao, X., Zhou, B., Wang, N., 2025. Driving mechanisms and threshold identification of landscape ecological risk: a nonlinear perspective from the Qilian Mountains, China. Ecol. Indic. 173, 113342. https://doi.org/10.1016/j.ecolind.2025.113342.

Ren, H., Liu, B., Zhang, Z., Li, F., Pan, K., Zhou, Z., Xu, X., 2022. A water-energy-food-carbon nexus optimization model for sustainable agricultural development in the Yellow River Basin under uncertainty. Appl. Energy 326, 120008. https://doi.org/10.1016/j.apenergy.2022.120008.

Shao, W., Zhang, Z., Guan, Q., Yan, Y., Zhang, J., 2024. Comprehensive assessment of land degradation in the arid and semiarid area based on the optimal land degradation index model. Catena 234, 107563. https://doi.org/10.1016/j.catena.2023.107563.

Shi, J., Zhang, P., Liu, Y., Tian, L., Cao, Y., Guo, Y., Li, J., Wang, Y., Huang, J., Jin, R., Zhu, W., 2024. Study on spatiotemporal changes of wetlands based on PLS-SEM and PLUS model: the case of the Sanjiang Plain. Ecol. Indic. 169, 112812. https://doi.org/10.1016/j.ecolind.2024.112812.

Shirmohammadi, B., Malekian, A., Salajegheh, A., Taheri, B., Azarnivand, H., Malek, Z., Verburg, H.P., 2020. Scenario analysis for integrated water resources management under future land use change in the Urmia Lake region, Iran. Land Use Policy 90, 104299. https://doi.org/10.1016/j.landusepol.2019.104299.

Song, X., Gao, Y., Wen, X., Guo, D., Yu, G., He, N., Zhang, J., 2017. Carbon sequestration potential and its eco-service function in the karst area, China. J. Geogr. Sci. 27, 967–980. https://doi.org/10.1007/s11442-017-1415-3.

Sweeting, M.M., 2012. Karst in China: Its Geomorphology and Environment. Springer.

Tang, T., Ge, J., Shi, H., Wang, L., Cao, J., Lee, X., 2025. Drought frequency, intensity, and exposure have increased due to historical land use and land cover changes. Commun. Earth Environ. 6, 398. https://doi.org/10.1038/s43247-025-02392-0.

Wang, R.Y., Cai, H., Chen, L., Li, T., 2023. Spatiotemporal evolution and multi-scenario prediction of carbon storage in the GBA based on PLUS-InVEST models. Sustainability 15, 8421. https://doi.org/10.3390/su15108421.

Wang, G., Han, Q., 2021. The multi-objective spatial optimization of urban land use based on low-carbon city planning. Ecol. Indic. 125, 107540. https://doi.org/10.1016/j.ecolind.2021.107540.

Wang, R.Y., Huang, G., Zi, P., Li, T., Liang, Q., 2025. Implementation of ecological risk scenario simulation and driving mechanisms in typical rocky desertification regions in China: a coupling multi-model ecological assessment framework. Ecol. Indic. 174, 113464. https://doi.org/10.1016/j.ecolind.2025.113464.

Wang, R.Y., Mo, X., Ji, H., Zhu, Z., Wang, Y.S., Bao, Z., Li, T., 2024. Comparison of the CASA and InVEST models' effects for estimating spatiotemporal differences in carbon storage of green spaces in megacities. Sci. Rep. 14, 5456. https://doi.org/10.1038/s41598-024-55858-0.

Wei, P., Du, J., Bahadur, A., Zhang, H., Wang, S., Wu, T., Chen, S., 2025. Soil erosion and risk assessment on the Qinghai-Tibetan Plateau. Commun. Earth Environ. 6, 365. https://doi.org/10.1038/s43247-025-02355-5.

Xiao, B., Bai, X., Zhao, C., Tan, Q., Li, Y., Luo, G., Wu, L., Chen, F., Li, C., Ran, C., Luo, X., Xi, H., Chen, H., Zhang, S., Liu, M., Gong, S., Xiong, L., Song, F., Du, C., 2023. Responses of carbon and water use efficiencies to climate and land use changes in China's karst areas. J. Hydrol. 617, 128968. https://doi.org/10.1016/j.jhydrol.2022.128968.

Yang, J., Zheng, J., Han, C.Q., Lu, B., Yu, W., Wang, Z., Wu, J., Han, L., 2025. Exploring suitable models for regional ecological development: a Study on multi-scenario ecological risk assessment in typical arid regions. Land Degrad. Dev. 36, 2815–2830. https://doi.org/10.1002/ldr.5533.

Yang, Y., Yuan, X., An, J., Su, Q., Chen, B., 2024. Drivers of ecosystem services and their trade-offs and synergies in different land use policy zones of Shaanxi Province, China. J. Clean. Prod. 452, 142077. https://doi.org/10.1016/j.jclepro.2024.142077.

Yu, P., Liu, J., Tang, H., Ci, E., Tang, X., Liu, S., Ding, Z., Ma, M., 2025. The increased soil aggregate stability and aggregate-associated carbon by farmland use change in a karst region of Southwest China. Catena 231, 107284. https://doi.org/10.1016/j.catena.2023.107284.

Yun, K., Zhang, M., Zhang, Y., 2024. Investigating the coupled coordination of improved ecological environment and socio-economic development in alpine wetland areas: a case study of southwest China. Ecol. Indic. 160, 111740. https://doi.org/10.1016/j.ecolind.2024.111740.

Zhao, Q., Zou, D., Chai, Z., Li, M., Yu, D., 2025. Effects of Land Use Change on the Temporal and Spatial Dynamics of Ecosystem Carbon Storage in the Wujiang River Basin, Guizhou, vol. 5. China Rural Water Hydropower, pp. 9–16. https://doi.org/10.12396/znsd.241284.

Zhao, G., Gao, H., Li, Y., Tang, Q., Woolway, R.I., Merder, J., Rosa, L., Michalak, A.M., 2025. Decoupling of surface water storage from precipitation in global drylands due to anthropogenic activity. Nat. Water 3, 80–88. https://doi.org/10.1038/s44221-024-00367-7.

Zhou, D., Xiao, J., Frolking, S., Zhang, L., Zhou, G., 2022. Urbanization contributes little to global warming but substantially intensifies local and regional land surface warming. Earths Future 10. https://doi.org/10.1029/2021EF002401 e2021EF002401.

Zhou, K., Zheng, X., Huang, S., Li, H., Yin, H., 2025. Quantifying the combined and individual impacts of climate and human activity on the urban green space carbon sink capacity in Beijing. Sustain. Cities Soc. 122, 106253. https://doi.org/10.1016/j.scs.2025.106253.